Biomech Model Mechanobiol
DOI 10.1007/s10237-015-0742-5

ORIGINAL PAPER

Investigating the effects of membrane deformability on artificial capsule adhesion to the functionalized surface

Hiren D. Balsara[1] · **Rohan J. Banton**[2] · **Charles D. Eggleton**[1]

Received: 15 April 2015 / Accepted: 26 October 2015

Abstract Understanding, manipulating and controlling cellular adhesion processes can be critical in developing biomedical technologies. Adhesive mechanisms can be used to the target, pattern and separate cells such as leukocytes from whole blood for biomedical applications. The deformability response of the cell directly affects the rolling and adhesion behavior under viscous linear shear flow conditions. To that end, the primary objective of the present study was to investigate numerically the influence of capsule membrane's nonlinear material behavior (i.e. elastic-plastic to strain hardening) on the rolling and adhesion behavior of representative artificial capsules. Specifically, spherical capsules with radius of 3.75 μm were represented using an elastic membrane governed by a Mooney–Rivlin strain energy functions. The surfaces of the capsules were coated with P-selectin glycoprotein-ligand-1 to initiate binding interaction with P-selectin-coated planar surface with density of 150 μm^{-2} under linear shear flow varying from 100 to 400 s^{-1}. The numerical model is based on the Immersed Boundary Method for rolling of deformable capsule in shear flow coupled with Monte Carlo simulation for receptor/ligand interaction modeled using Bell model. The results reveal that the mechanical properties of the capsule play an important role in the rolling behavior and the binding kinetics between the capsule contact surface and the substrate. The rolling behavior of the strain hardening capsules is relatively smoother and slower compared to the elastic-plastic capsules. The strain hardening capsules exhibits higher contact area at any given shear rate compared to elastic-plastic capsules. The increase in contact area leads to decrease in rolling velocity. The capsule contact surface is not in complete contact with the substrate because of thin lubrication film that is trapped between the capsule and substrate. This creates a concave shape on the bottom surface of the capsule that is referred to as a dimple. In addition, the present study demonstrates that the average total bond force from the capsules lifetime increases by 37 % for the strain hardening capsules compared to elastic-plastic capsules at shear rate of 400 s^{-1}. Finally, the model demonstrates the effect of finite membrane deformation on the coupling between hydrodynamic and receptor/ligand interaction.

Keywords Adhesion mechanics · Capsule deformation · Immersed boundary method · Monte Carlo simulation · Leuko-polymersomes

1 Introduction

Adhesion mechanics plays an important role in many processes involving artificial microcapsules and biological cells. Artificial microcapsules have been used in many industries including the cosmetics (Magill 1990; Miyazawa et al. 2000) and food and pharmaceutical industry (Soda et al. 1989; Vallner et al. 1983; Nimmerfall and Rosenthaler 1986). The main role or function of these artificial capsules is to deliver their encapsulated content to targeted sites through the binding interactions between the targeted surface and the microcapsule (Devarajan and Jain 2015). Understanding, manipulating and controlling adhesion (binding) processes are crucial to developing strategies and technologies involving the usage of artificial microcapsules.

✉ Charles D. Eggleton
eggleton@umbc.edu

[1] Department of Mechanical Engineering, University of Maryland, Baltimore County, Baltimore, MD 21250, USA

[2] US Army Research Laboratory, Aberdeen Proving Ground, Aberdeen, MD, USA

Published online: 13 November 2015

Artificial microcapsules such as polymersomes with the adhesion properties of leukocytes, which is referred to as Leuko-polymersomes, were designed by Hammer et al. (2008), Robbins et al. (2010). Polymersomes make an ideal choice for drug delivery carriers because of their tunable membrane properties as well as their ability to encapsulate a broad range of drugs (Lee and Feijen 2012; Discher et al. 2002). Polymersomes are made using amphiphilic synthetic block copolymers, whose mechanical properties are tuned by varying the composition and molecular weight (Bermudez et al. 2002; Lee and Feijen 2012). Hammer et al. (2008) were able to demonstrate that Leuko-polymersomes can adhere specifically to the substrate and measured adhesion at shear rates of $130\,s^{-1}$. The researchers were able to coat up to two different molecules on the surface of the polymersomes (Hammer et al. 2008).

Polymersome was chosen to mimic the leukocyte because leukocyte exhibits cellular adhesive behavior throughout the vasculature system. The cellular adhesion is manifested through the processes of leukocyte rolling to the sites of inflammation. These biological processes typically involve three main steps: (1) cells are captured from the blood stream through bond formation between the cell and vessel wall; (2) the cell is able to roll along the surface of the vessel wall by forming bonds at the leading edge of the cell while breaking bonds at the rear of the cell; and (3) the cell is able to tightly adhere to the surface and transmigrate across the endothelium (Lawrence and Springer 1991; Dong and Lei 2000; Dore et al. 1993).

The leukocyte rolling has been extensively studied in both in vivo and in vitro settings (Alon and Ley 2008; Hyduk and Cybulsky 2009; Norman et al. 1995; Smith et al. 2002; Petri et al. 2008) where the influence of the binding kinetics of receptor–ligand bond formation as well as wall shear rate has been demonstrated to affect the rolling behavior of leukocyte.

Numerical models have provided significant insight into the leukocyte rolling and binding. The first adhesion dynamics (AD) model was developed by Hammer and Apte (1992). AD was used to capture the binding kinetics interactions between the leukocytes rolling on a selectin-coated hard surface. In AD, the leukocyte was modeled as a rigid sphere with rigid microvilli (Hammer and Apte 1992). The AD was able to recreate the transient "stop and go" motion of the leukocyte and calculate the translational velocity. The AD model has been used to study the effects of different parameters such as bond properties and the number of receptors on microvillus tips among others. Caputo and Hammer (2005) used AD to study the effect of microvillus deformability on leukocyte adhesion and found that stiffer microvilli result in faster rolling.

In addition to AD, Tözeren and Ley (1992) modeled the leukocyte as a rigid sphere with membrane folds and other unspecified surface projections. They found that the leukocyte rolling was influenced by the bond length and local cell stiffness near the bond. Other works, (Khismatullin and Truskey 2005), modeled the leukocyte as a compound viscoelastic drop with the receptor–ligand interaction modeled using spring-peeling kinetic model. Khismatullin and Truskey found that for a constant wall shear rate, the cell–substrate contact area and shear force acting on the cell increased as the chamber height decreased (Ley 2009).

More recently, leukocyte rolling and adhesive models also included the deformability of the whole cell (Jadhav et al. 2005; Pappu et al. 2008; Pawar et al. 2008; Gupta et al. 2010). These models represented the leukocytes as a microcapsule filled with a Newtonian fluid enclosed by a thin hyperelastic membrane. A neo-Hookean constitutive relations was used to characterize the behavior of the hyperelastic cell membrane, while the Hookean springs approach was used to represent the receptor–ligand interaction of the microcapsule with selectin-coated hard surfaces.

Rachik et al. (2006) conducted compression test on microcapsule and numerically modeled the experiment using various constitutive relation such as neo-Hookean, Mooney–Rivlin (MR), and Yeoh. The authors concluded that MR constitutive equation accurately described the experimental results (Rachik et al. 2006). The microcapsule was made of alginate cross-linked with human serum albumin using process developed by Edwards-Lévy and Lévy (1999) and the microcapsule radii ranged from 1.55 to 1.42 mm.

From the above-mentioned studies (Alexeev et al. 2006; Jadhav et al. 2005; Rachik et al. 2006), it became apparent that the cell deformability plays a significant role in tethering, rolling and more importantly the adhesive (binding) kinetics of microcapsules/biological cells to targeted sites or surface substrate. The primary objective of this work was to investigate numerically the influence of cell membranes nonlinear material behavior (i.e. elastic-plastic to strain hardening) on the rolling and adhesion behavior of representative artificial cells. The capsule's hyperelastic membrane was modeled using a Mooney–Rivlin constitutive law, which is most often used to model the elastic response of a rubber-like material Mooney (1940) and Rivlin (1948). Rubber is essentially a cross-linked polymer, whose mechanical properties can be influenced by the degree of cross-linking.

In the present work, the immersed boundary method (IBM) with finite element method (FEM) using MR constitutive law and Monte Carlo model for receptor ligand interaction was used to study the influence of strain hardening on capsule deformation, rolling, and binding kinetics. The influence of nonlinear material property was analyzed by varying Γ value from zero to one in the MR strain energy density function to span elastic-plastic to strain hardening behavior.

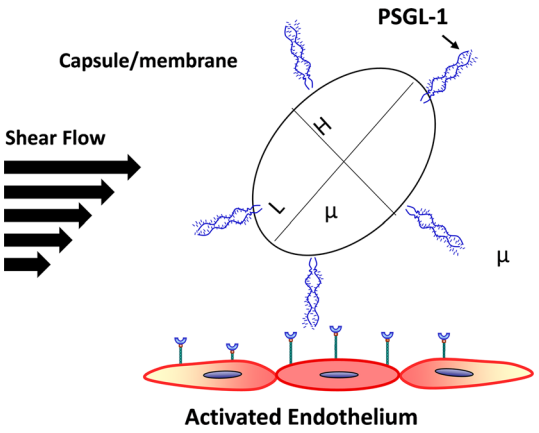

Fig. 1 Schematic of an artificial capsule coated with P-selectin glycoprotein-ligand-1 (PSGL-1) rolling on an endothelium under shear flow. The capsule deformation due to shear flow is represented in terms of deformation index (L/H) where L and H are the length and height of the deformed cell, respectively. The encapsulated and external fluid viscosity is represented by μ

2 Computational model

Figure 1 shows a segmented portion of the problem geometry under consideration with a deformable spherical capsule binding to the bottom substrate under shear flow condition. Here the rolling adhesion of an elastically deformable spherical capsule, decorated with a rigid microvilli, is shown binding onto a P-selectin-coated plane surface in a microchannel. The full computational domain includes both the top and bottom parallel plates with a capsule subjected to a shear flow condition. The computational model is developed by combining: (1) the immersed boundary method to solve the Navier-Stokes equation for the motion of an elastic capsule near a plane in a linear shear flow (Eggleton and Popel 1998; Jadhav et al. 2005); (2) the finite element method to solve the constitutive equation for the MR membrane of the spherical capsule; and (3) the Monte Carlo method for simulating the formation and breakage of receptor–ligand bonds with kinetic rate constants based on the Bell model (Bell 1978).

2.1 Immersed boundary method

Initially, the immersed boundary method (IBM) was developed to study the fluid dynamics of heart valves by Peskin (1989). In the present work, the IBM has been adopted to model a 3-D elastic capsule containing a Newtonian fluid, where the motion of the fluid inside and outside of the elastic capsule is governed by the following continuity (Eq. 1) and Navier-Stokes (Eq. 2) equations:

$$\nabla \cdot u(\mathbf{x}, t) = 0 \tag{1}$$

$$\rho \frac{\partial u(\mathbf{x}, t)}{\partial t} = -\nabla p(\mathbf{x}, t) + \mu \nabla^2 u(\mathbf{x}, t) + \mathbf{F}(\mathbf{x}, t) \tag{2}$$

which are discretized by finite differencing on a uniform Cartesian grid; ρ and μ are the density and viscosity of the fluid inside and outside of the capsule membrane, respectively; $u(\mathbf{x}, t)$ and $p(\mathbf{x}, t)$ are the velocity and pressure, respectively, at fluid grid nodes $\mathbf{x}(x, y, z)$ at time t. In addition, $\mathbf{F}(\mathbf{x}, t)$ is the total force acting at each fluid grid nodes and comprises of the forces exerted by the plane, elastic capsule, and receptor–ligand bonds.

In the IBM, the computational domain is composed of an Eulerian Cartesian fluid grid nodes $\mathbf{x}(x, y, z)$ and a Lagrangian triangular finite element grid $\mathbf{X}(X, Y, Z)$ that tracks the capsule deformation and motion (Jadhav et al. 2005; Pawar et al. 2008). At the start of each time step t, the forces that arise from the restoring forces due to the deformation of elastic elements of the capsule and the adhesion forces due to bond formation between the receptor–ligand are computed. These forces are denoted as $\mathbf{F}(\mathbf{X}, t)$, which acts on the capsule surface. These forces are related to the total fluid force $\mathbf{F}(\mathbf{x}, t)$, which acts on the fluid nodes through the following relation:

$$\mathbf{F}(\mathbf{x}, t) = \sum \mathbf{F}(\mathbf{X}, t) \cdot D_h(\mathbf{X} - \mathbf{x}) \text{ for } |\mathbf{X} - \mathbf{x}| \leq 2h \tag{3}$$

The forces, $\mathbf{F}(\mathbf{X}, t)$, are distributed from a point on a capsule surface to the fluid grid nodes using an appropriately chosen function $D_h(\mathbf{X} - \mathbf{x})$, which vanishes everywhere except at the membrane, as shown in Eq. (4).

$$D_h(\mathbf{X} - \mathbf{x}) = \delta_h(X_1 - x_1)\delta_h(X_2 - x_2)\delta_h(X_3 - x_3) \tag{4}$$

where h is the uniform grid spacing and the 3-D discrete δ-function is expressed as:

$$\delta_h(z) = \begin{cases} \frac{1}{4h}\left(1 + \cos(\frac{\pi \cdot z}{2h})\right) & \text{for } |z| \leq 2h \\ 0 & \text{for } |z| > 2h \end{cases} \tag{5}$$

The Navier-Stokes and continuity equations are first solved to obtain the fluid velocity and pressure in the entire fluid domain by first discretizing the fixed Eulerian grid, $\mathbf{x}(x, y, z)$. Periodic boundary conditions are imposed on the velocity and pressure, and fast Fourier transform method is implemented to solve the flow equation (Peskin 1989; Jadhav et al. 2005; Pawar et al. 2008). In addition, the no slip boundary condition at the elastic capsule membrane surface and the stationary plane are enforced by moving their respective nodes with the local fluid velocity. The velocity of the capsule membrane, $\mathbf{U(X, t)}$, is computed from the velocity at fluid gird node, $\mathbf{u(x, t)}$, using the δ-function, using the same approach used for total force:

$$\mathbf{U}(\mathbf{X}, t) = \sum \mathbf{u}(\mathbf{x}, t) \cdot D_h(\mathbf{X} - \mathbf{x}) \text{ for } |\mathbf{X} - \mathbf{x}| \leq 2h \tag{6}$$

At the end of each time step, the position of the membrane nodes and the plane are updated with the following relation,

$$\mathbf{X}_{t+\Delta t} = \mathbf{X}_t + \Delta t U_{t+\Delta t}(\mathbf{X}_t) \tag{7}$$

2.2 Capsule membrane constitutive equation

The elastic membrane of the capsule is assumed to have a stress-free shape initially, which is discretized into flat triangular elements. The MR form of the strain energy density function, which is assumed to be incompressible and initially isotropic, describes the capsules membrane mechanics. This strain energy function, W, is expressed as a function of only the in-plane principal stretch ratios, λ_1 and λ_2,

$$W = \frac{Eh}{6}\left[(\lambda_1^2 + \lambda_2^2 + \lambda_1^{-2}\lambda_2^{-2} - 3) + \Gamma(\lambda_1^2\lambda_2^2 + \lambda_1^{-2} + \lambda_2^{-2} - 3)\right] \tag{8}$$

where E is Youngs modulus for the elastic material, h is the membrane thickness, and Γ is a dimensionless constant. When Γ is equal to zero in Eq. (8), the strain energy function for neo-Hookean membrane material is obtained. By using the principal of virtual work, the relationship between the nodal displacement and nodal forces are obtained. These in-plane forces at the vertices of each flat triangular element are computed using the finite difference procedure outlined in Charrier et al. (1989) and Eggleton and Popel (1998).

2.3 Monte Carlo simulation for bond formation and rupture

The binding kinetics of receptor–ligand interactions that results in bond formation and/or rupture from the capsule rolling on the selectin-coated surface is captured using the Bell model (Bell 1978). According to the Bell model, the forward and reverse rate constants for the receptor–ligand interaction are given by:

$$k_f = k_f^0 \exp\left[\frac{\sigma_b|L_b - L_{b0}|\left(x_\beta - \frac{1}{2}|L_b - L_{b0}|\right)}{k_B T}\right] \tag{9}$$

$$k_r = k_r^0 \exp\left[\frac{x_\beta F}{k_B T}\right] \tag{10}$$

where k_f^0 and k_r^0 are the forward and reverse rate constants at the equilibrium distance L_{b0}; $k_B T$ is the thermal energy; F is the force acting on the bond; σ_b is the spring constant in the bound state; and x_β is the reactive compliance. The reactive compliance is a parameter that has the units of length, which determines the degree to which force facilitates bond breakage. The force acting on the bond, F, is determined by:

$$F = \sigma_b(L_b - L_{b0}) \tag{11}$$

The stochastic nature of the receptor–ligand interactions is included in the Monte Carlo simulation. The probability that a receptor will bind, P_f, and that an existing bond rupture, P_r, are given by Hammer and Apte (1992) for a given time interval, Δt,

$$P_f = 1 - \exp(-k_{\text{on}}\Delta t) \tag{12}$$

$$P_r = 1 - \exp(-k_r \Delta t) \tag{13}$$

where $k_{\text{on}} = k_f A_L(n_L - n_B)$. A_L is the surface area on the ligand-coated plane accessible to each receptor, and $(n_L - n_B)$ is the density of unbound ligand. At a given time, the probabilities of bond formation and rupture are compared to two random numbers generated P_{ran1} and P_{ran2}, which are between 0 and 1. If P_f is greater than P_{ran1}, then the bond has formed, whereas P_r less than P_{ran2} dictates that the bond has ruptured. A time step of 10^{-6} s was used to simulate the capsule rolling for a period of 1 s. In addition, the microvilli are modeled as solid cylinders that does not deform under force. Finally, it is important to note that the IBM does not account for the roughness caused by the microvilli in the simulation to capture the motion of an elastic capsule.

3 Results

Simulations of the rolling adhesion of capsule, decorated with PSGL-1 molecules localized on the tips of solid microvilli, over P-selectin-coated surface in a shear flow using a 3-D computational model based on IBM are performed. As a first step, the computational model is validated by computing the rolling velocity for the model described by Jadhav et al. (2005) with a membrane stiffness value of 0.3 dyn/cm. The computational model outlined in Jadhav et al. (2005) uses a neo-Hookean membrane material, which is characterized in the present model by using a MR membrane material with the same membrane stiffness and with Γ set to zero. The Dembo model utilized by Jadhav et al. (2005) is reinstructed in the present model to represent the receptor–ligand interactions for the validation purposes only. Figure 2 represents the rolling velocity computed using the present model compared with data presented in Jadhav et al. (2005). The results vary by <5 % with the previously published data, and the slight discrepancy is due to the stochastic nature of the receptor–ligand interaction.

3.1 Capsule membrane deformability under static loading

To gain further insight into the effect of the membrane deformability on the rolling and binding kinetics of the capsule, it was first necessary to examine and evaluate the

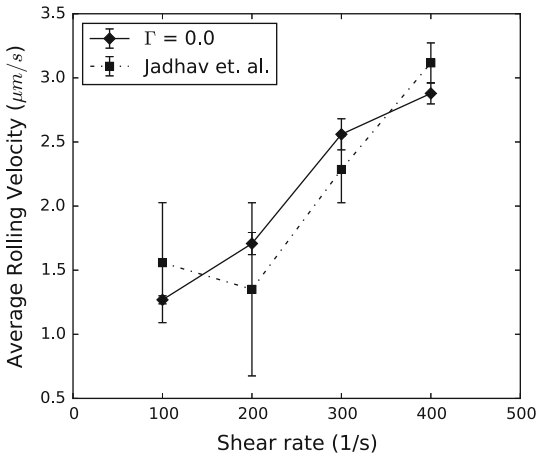

Fig. 2 Average rolling velocity of a deformable spherical capsule as a function of shear rate. The average rolling velocity was estimated as a function of shear rate from the simulations using the IBM for a spherical capsule with radius of 3.75 μm, membrane stiffness value *Eh* of 0.3 dyn/cm, dimensionless parameter $\Gamma = 0.0$. This represents a neo-Hookean membrane constitutive model. The average rolling velocity of a deformable spherical capsule of same size and using same parameter as simulated by Jadhav et al. (2005) (mean ± SE; $n = 3$–5)

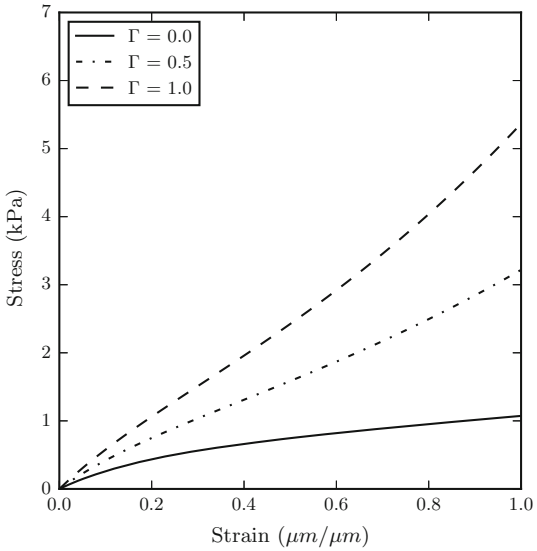

Fig. 3 Stress–strain curve generated by gradually inflating the sphere by increasing the radius and using the finite element solver that incorporated the Mooney–Rivlin strain energy function to compute the forces on each elements of the shell, where $Eh = 0.3$ dyn/cm and $\Gamma = 0.0$, 0.5, and 1.0 at a given moment

behavior of the membrane itself under static loading conditions. This evaluation of the membrane was carried out by considering the classical problem of inflation of a thin spherical shell which initially has a stress-free shape (Green 1970). Here the membrane was likened to a stress-free spherical shell that was then inflated by gradually increasing the radius. A finite element solver was used to compute the forces on each elements of the shell. At the inflated state, the strain was considered constant and the amount of forces exerted on each element was also constant. From these results, stress–strain curves was generated for the various values of the dimensionless parameter, Γ. Here Γ is varied from zero to one with the parameter *Eh* held fixed at 0.3 dyn/cm. It is noticed that as the value of Γ is increased, there is a strain hardening effect in the stress response curves at large strain (see Fig. 3). Initially, the modulus of elasticity for all three values of Γ is within 7 % of each other for strains less than 0.1. At larger strains (>0.1), the membrane stress increases in the nonlinear regime as the parameter, Γ, increases. It should be noted, however, that in the case of the neo-Hookean membrane defined as Γ equal to zero, there was minimal increase in stress over prolonged increase in strain. This condition is representative of a strain softening material.

3.2 Capsule membrane deformability under shear loading

Next, simulations were performed for capsule rolling over a P-selectin-coated surface in a shear flow using the parameter values in Table 1. The capsule deformation was quantified as previously reported in the literature (Smith et al. 2002; Jadhav et al. 2005), by the deformation index, *L/H*, where *L* was the average length in the direction of the flow and *H* was the height of the capsule.

In the present study, the deformation index, *L/H*, increases with the shear rate for the capsule with the most compliant membrane ($\Gamma = 0$; see Fig. 4a). For capsules with strain hardening membranes (i.e. Γ values of 0.5 and 1.0), the increase in deformation index with increasing shear rate is less proclaimed (see Fig. 4a). The results indicate that increase in the membrane stiffness produced decrease in membrane deformability, *L/H*, across all shear rates. Figure 4b shows the corresponding capsule profile at shear rate of 100 and 400 s^{-1}, respectively. There is a common flattening of the spherical capsule in the region proximate to the plane for the entire range of shear rates considered. This is evident for both shear rates shown in Fig. 4. At low shear rate of 100 s^{-1}, an almost spherical capsule shape was maintained for all three Γ values. At the higher shear rate of 400 s^{-1}, the capsules exhibited an increasing deviation from the spherical shape, with the capsule having the most compliant membrane ($\Gamma = 0$) displaying the largest deviation among the three values of Γ. At the higher values of Γ, the capsules exhibited less elongation in the direction of the flow.

Figure 5 represents the average capsule–substrate contact area as a function of the shear rate. The difference in contact area among the various values of Γ is <15 % for a given shear rate. For high shear rate of 400 s^{-1}, the strain hardening membrane had higher contact area than strain softening membrane.

Table 1 Numerical values of parameter used in the simulation (unless otherwise noted)

Parameter	Definition	Value	References
R	Capsule radius	3.75 μm	Tandon and Diamond (1998)
L_{mv}	Length of microvillus	0.35 μm	Shao et al. (1998)
N_{mv}	No. microvilli/capsule	252	Chen and Springer (1999)
N_{Lmv}	No. PSGL-1 mol/microvillus	50	Moore et al. (1991)
N_R	P-selectin (receptor) site density	150 μm^{-2}	Yago et al. (2004)
x_β	Reactive compliance	0.03 nm	Caputo and Hammer (2005)
L_{b0}	Equilibrium bond length	0.1 μm	Fritz et al. (1998)
k_r^0	Unstressed off-rate	1 s^{-1}	Mehta et al. (1998)
k_f^0	Unstressed on rate	1 s^{-1}	Mehta et al. (1998)
σ_b	Bond spring constant	1 dyn/cm	Dembo (1994)
σ_{ts}	Transition state spring constant	0.99 dyn/cm	Dembo (1994)
Eh	Membrane stiffness	0.3 dyn/cm	Jadhav et al. (2005)
Γ	Membrane's nonlinear stiffness (dimensionless) parameter	0–1.0	
Γ	Shear rate	100–400 s^{-1}	Jadhav et al. (2005)
μ	Fluid viscosity	0.8 cp	
ρ	Fluid density	1 g/cc	
T	Temperature	310 K	

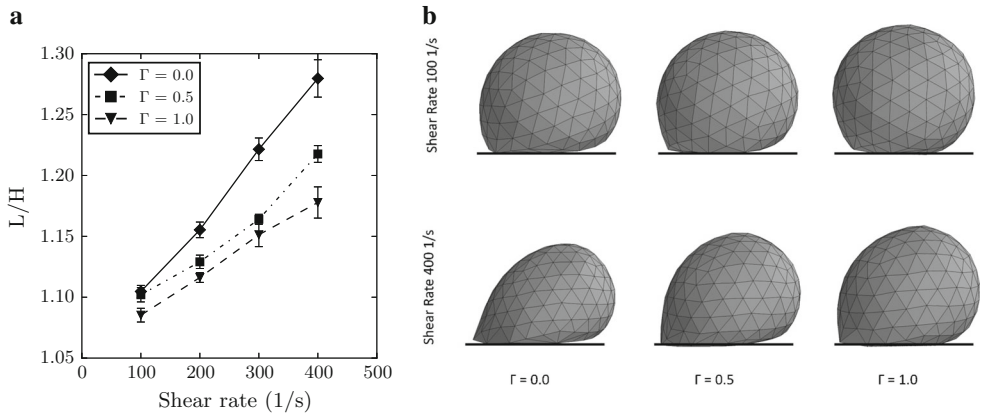

Fig. 4 **a** Capsule deformation during rolling as a function of shear rate using parameter listed in Table 1. The average length/height ratio (L/H) was computed using the IBM simulation for a capsule rolling under shear flow condition on a selectin-coated plane. The shear rate varied from 100 to 400 s^{-1} for Γ values of 0.0, 0.5 and 1.0 (mean ± SE; $n = 5$–7) **b** The representative capsule shapes at shear rate of 100 and 400 s^{-1} are shown for fixed membrane stiffness value (Eh) of 0.3 dyn/cm with varying Γ values of 0.0, 0.5, and 1.0

Figure 6 depicts a snapshot of the contact area at a single time step at shear rate of 100 and 400 s^{-1}, respectively. Overlaid on the contact area is the contour of forces acting on each node. The total force is due to the elastic restoring force and receptor–ligand bond force. At the shear rate of 100 s^{-1}, there is more contact between the rear of the capsule and the substrate for a given membrane's nonlinear stiffness (dimensionless) parameter, Γ. As the degree of strain hardening increases (i.e. $\Gamma > 0$), the total forces acting on the node also increases, which is evident from changes in the color map. The higher forces are concentrated on the rear of the capsule for all values of the dimensionless parameter, Γ.

At the shear rate of 400 s^{-1} and Γ equal to zero, the contact area between the capsule and substrate is mostly circumferential with the middle region filled with the same fluid that encompass the capsule. As the membrane become more strain hardening (i.e. $\Gamma > 0$), greater contact area is produced at the front of the capsule with the substrate. In contrast, the strain hardening membrane produced more contact in the center with the substrate compared to a neo-Hookean membrane (i.e. $\Gamma = 0$). Overall, the total forces acting on the node increases with the increase in degree of strain hardening. This was also observed at shear rate of 100 s^{-1}.

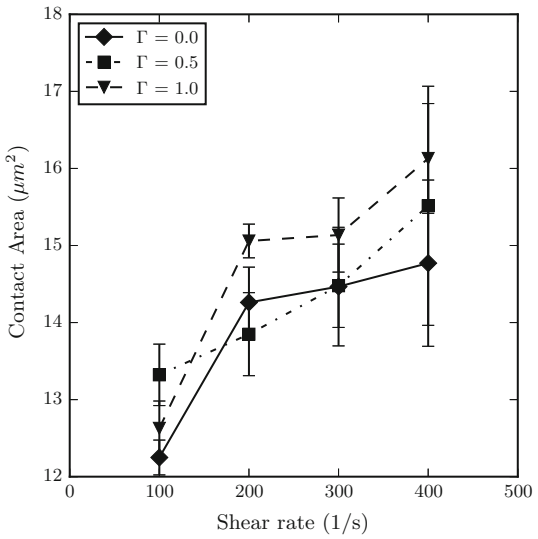

Fig. 5 Average capsule–substrate contact area as a function of the shear rate was estimated from IBM simulations for a deformable capsule rolling under shear flow conditions. The shear rates varied from 100 to 400 s^{-1} for Γ values of 0.0, 0.5, and 1.0 (mean ± SE; $n = 5$–7)

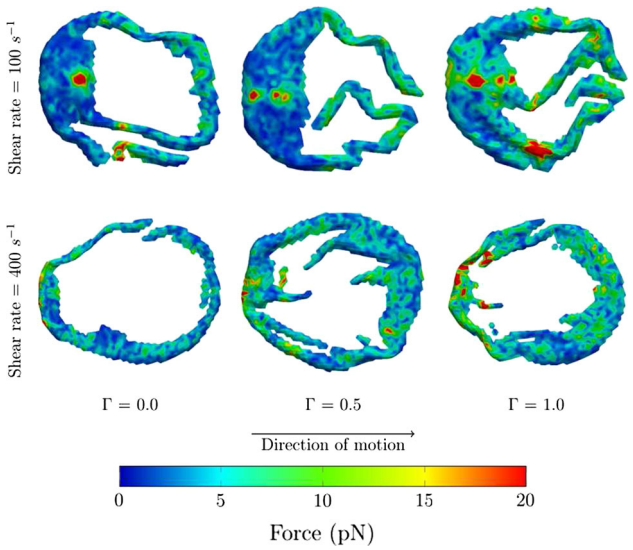

Fig. 6 Contact area shapes at shear rate of 100 and 400 s^{-1} are shown for fixed membrane stiffness value (Eh) of 0.3 dyn/cm with varying Γ value of 0.0, 0.5, and 1.0

Figure 7 shows the contact area shapes overlaid for shear rate of 100 and 400 1/s with varying gamma values of 0.0, 0.5, and 1.0. The contact area only increased by <15 % as the shear rate increased from 100 to 400 s^{-1}; however, the footprint of the contact area is significantly higher for the shear rate of 400 s^{-1} compared to 100 s^{-1}. The higher shear rate caused the capsule to deform more, which lead to the capsule having a higher footprint. The contact area of the capsules at the specific shear rate of 400 s^{-1} with the various values of Γ was overlaid and presented in Fig. 8. The neo-Hookean membrane (i.e. $\Gamma = 0$) has a bigger footprint compared to a

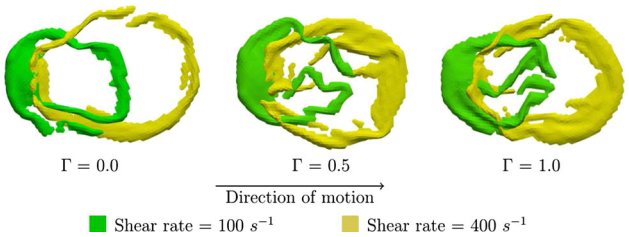

Fig. 7 Contact area shapes are overlaid for shear rate of 100 and 400 s^{-1} with varying Γ value of 0.0, 0.5, and 1.0

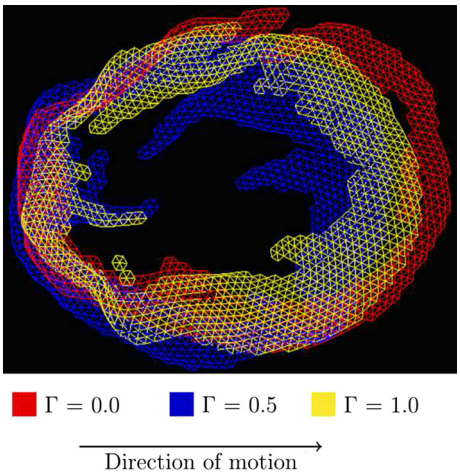

Fig. 8 Contact area shapes are overlaid for Γ value of 0.0, 0.5, and 1.0 at shear rate of 400 s^{-1}

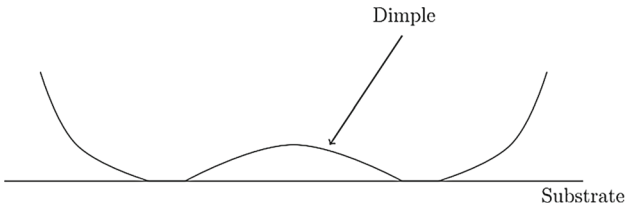

Fig. 9 Schematic of the contact area shape from the side view representing the concave shape that forms underneath the capsule (not drawn to scale)

strain hardening membrane; Γ value of 1.0 has bigger footprint than Γ value of 0.5, which has more contact area in the center compared to the other values of Γ.

A concave shape forms on the underside of the capsule that is not touching the substrate thus producing a dimple in the capsule underbelly. The schematic of a dimple is represented in Fig. 9. To illustrate that a dimple exists, a snapshot in time is taken of a capsule with Γ value of 0 at shear rate of 400 s^{-1} from multiple viewpoint and shown in Fig. 10. The concave shape is present on the bottom surface of the capsule, and there are ridges that appear underneath the capsule. The concave shape is not perfectly smooth, but it is pronounced. This shape is observed for all of the capsules, which are not in complete contact with the substrate.

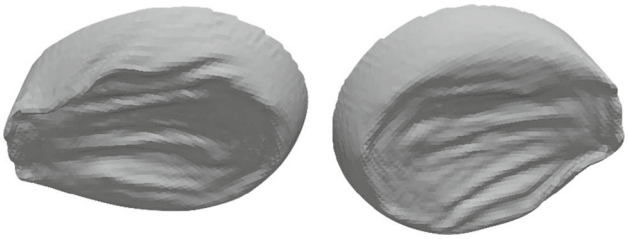

Fig. 10 Formation of a dimple on the bottom of the capsule with Γ value of 0.0 at shear rate of 400 s^{-1}. The snapshot of the same capsule, but from two different viewpoints

To further understand the strain hardening effects on the rolling behavior of the capsules, the instantaneous rolling velocity, average rolling velocity, the bond life time, the total bond force, and contact area shapes and sizes were analyzed. Figure 11a shows the instantaneous rolling velocity of the capsules as a function of the shear rate. The more compliant capsule ($\Gamma = 0.0$) had more fluctuations in the instantaneous rolling velocity, whereas the capsule with strain hardening membrane ($\Gamma = 1.0$) was relatively stable at shear rate of 400 s^{-1} (see Fig. 11a). At times, the instantaneous rolling velocity resulted in negative values with respect to the direction of flow due to oscillations in forces caused by the elastic response of the membrane. To analyze the rolling stability, the variance defined as $\frac{\sum_{i=1}^{n}(X_i-\bar{X})^2}{n-1}$ is recorded for instantaneous velocity of the capsules with various values of Γ as a function of shear rate. The variance in velocity decreases with increasing values of Γ over the entire range of shear rates examined (see Fig. 11b). This revealed relatively uniform rolling velocity for the strain hardening membrane ($\Gamma = 1.0$).

Figure 12 shows the effect of the Γ on the average rolling velocity of the capsules. At low shear rate of 100 s^{-1}, the variance in the average rolling velocity is <20 % between the three values of Γ for the capsule. However, there was a significant difference at higher shear rates among the various values of Γ. The average rolling velocity for the capsule with the strain hardening membrane ($\Gamma = 1.0$) had lower rolling velocity compared to the compliant membrane ($\Gamma = 0.0$) at high shear of 400 s^{-1} by at least 12 %. On the other hand, the average rolling velocity increased by at least 50 % from shear rate of 100 to 400 s^{-1} for all capsules with varying values of Γ (see Fig. 12).

The average number of receptor–ligand bonds was recorded as a function of shear rate for capsules with various degrees of strain hardening behavior. The simulated results indicated that the average number of bonds per capsule increased with the shear rate for all three values of Γ as shown in Fig. 13a. However, the increase in the average number of bonds with shear rate was not pronounced for any of the capsules. Indeed, the increase in average number of bonds was <25 % for all capsules when the shear rate was increased from 100 to

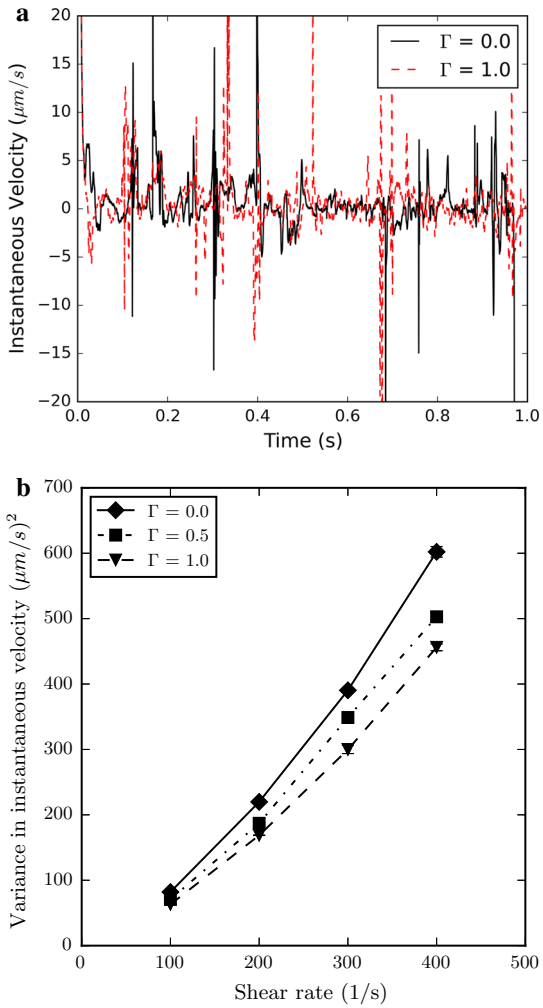

Fig. 11 Effect of transition from strain softening to strain hardening on the instantaneous velocity of the rolling capsules in shear flow. **a** The instantaneous rolling velocity of the capsule at shear rate of 400 s^{-1} was computed for Γ values of 0.0 and 1.0 as membrane transitions from strain softening to strain hardening, respectively. **b** The variance in the instantaneous capsule rolling velocity was estimate at shear rates varying from 100 to 400 s^{-1} for dimensionless parameter (Γ) values of 0.0, 0.5, and 1.0 (mean ± SE; n = 5–7)

400 s^{-1} (see Fig. 13a). In addition, the total receptor–ligand bond force experienced by the capsules at high shear rate of 400 s^{-1} more than doubled compared to shear rate of 100 s^{-1} for the capsules with Γ of 0 and 0.5, respectively, as shown in Fig. 13b). Additionally, there was <50 % difference among the capsules experiencing total bond force at high shear rate of 400 s^{-1}, whereas there is a difference of 100 % at low shear rate of 100 s^{-1} (Fig. 13b). The total bond force experienced by the capsules increased as the value of Γ increased for a given shear rate. To understand the influence of the total bond force on the receptor–ligand interaction kinetics, the average lifetime of PSGL-1 bonds were estimated from the simula-

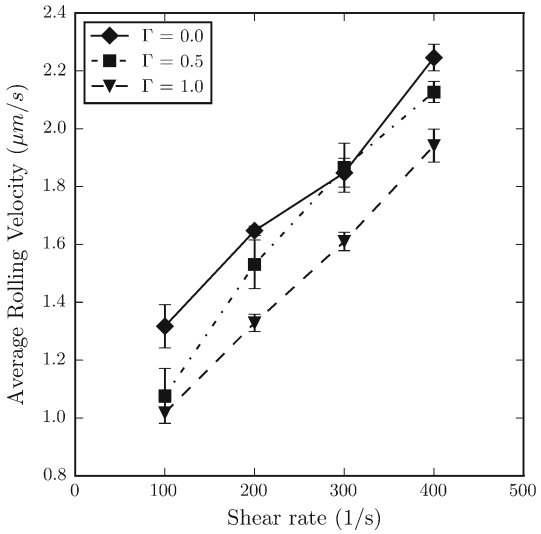

Fig. 12 Effect of strain hardening on the average rolling velocity of the capsules in shear flow. The average rolling velocity of capsule was calculated at shear rates of 100 to 400 s^{-1} for Γ values of 0.0, 0.5, and 1.0 (mean ± SE; $n = 5$–7)

tions. The data indicated that the average bond lifetime was 0.35 ± 0.02 s for all of the capsules as shown in Fig. 14.

3.3 Capsule binding kinetics under shear flow

Next, simulations were performed to investigate the effect of the unstressed reverse rate constant (off-rate) in the Bell model on the rolling velocity and the number of bonds formed in the lifetime of 1s. Figure 15 shows the average rolling velocity for the off-rate constant k_r^0 of 1, 5, and 10 s^{-1} with the shear rate of 400 s^{-1}. Increasing the off-rate resulted in shorter bond lifetime, thus leading to higher rolling velocity. The increase in rolling velocity was more than 60 % for the off-rate of 10 s^{-1} compared to 1 s^{-1} for all values of Γ. The rolling velocity is higher for less strain hardening membrane and the difference among the various values of Γ is <10 %.

Next, the average capsule–substrate contact area as a function of the off-rate constant, k_r^0, was analyzed and is represented in Fig. 16. The contact area for the neo-Hookean membrane (i.e. $\Gamma = 0.0$) decreased by <10 % as the off-rate constant increased from 1 to 5 s^{-1}; however, the contact area increased by <5 % as the off-rate constant increased from 5 to 10 s^{-1}. Similar trend was observed for the Γ value of 0.5, where the initial decrease was <5 % from off-rate constant of 1 to 5 s^{-1}, but contact area increased by 17 % from off-rate constant of 5 to 10 s^{-1}. On the other hand, the contact area increased as the off-rate constant increased for the strain hardening membrane (i.e. $\Gamma = 1.0$). The rolling velocity of the capsule was not impacted by the increase in the contact area.

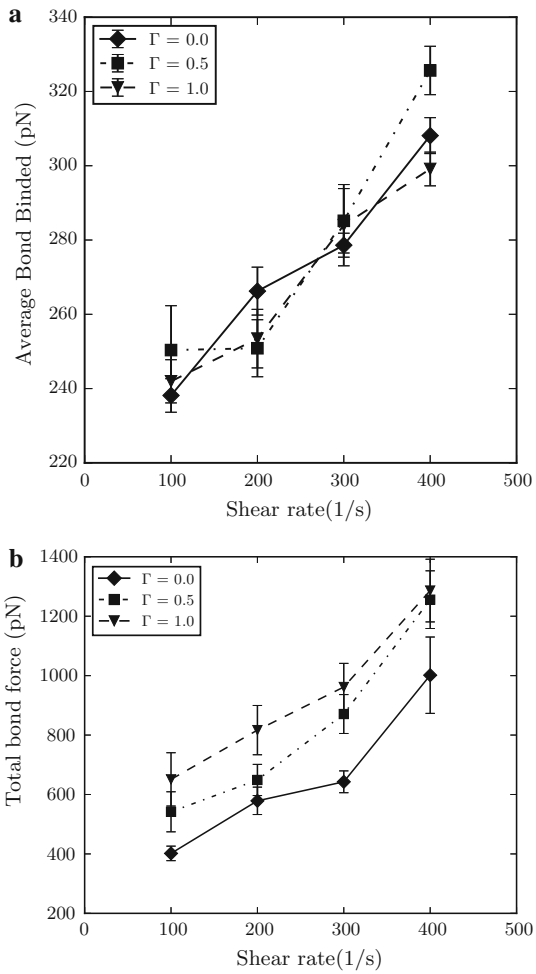

Fig. 13 Average number of instantaneous receptor–ligand bonds and the total bond force function of shear rate. **a** The average number of instantaneous receptor–ligand bonds during capsule rolling on selectin-coated plane was calculated at shear rates of 100 to 400 s^{-1} for dimensionless parameter (Γ) values of 0.0 and 1.0. **b** The time-averaged value of total receptor–ligand bond force acting on the capsule was calculated at shear rates of 100 to 400 s^{-1} for dimensionless parameter (Γ) values of 0.0, 0.5, and 1.0 (mean ± SE; $n = 5$–7)

To further analyze why the capsule with higher velocity also had higher contact area, a snapshot of the contact area shapes for the off-rate constant of 5 and 10 s^{-1} with fixed shear rate of 400 s^{-1} and with various values of Γ was taken and is presented in Fig. 17. There is more contact between the front of the capsule and the substrate for off-rate constant, k_r^0, of 10 s^{-1} for all values of Γ. The total forces acting on the nodes were higher for k_r^0 of 5 s^{-1} compared to k_r^0 of 10 s^{-1} for any given value of Γ (see Fig. 17).

Figure 18 shows the number of bonds that were formed in the lifetime of 1s as the values of the off-rate were varied. The number of bonds that formed in the lifetime increased by 650 % as k_r^0 increased from 1 to 10 s^{-1}. In addition, the strain hardening membrane formed at least 7 % more bonds

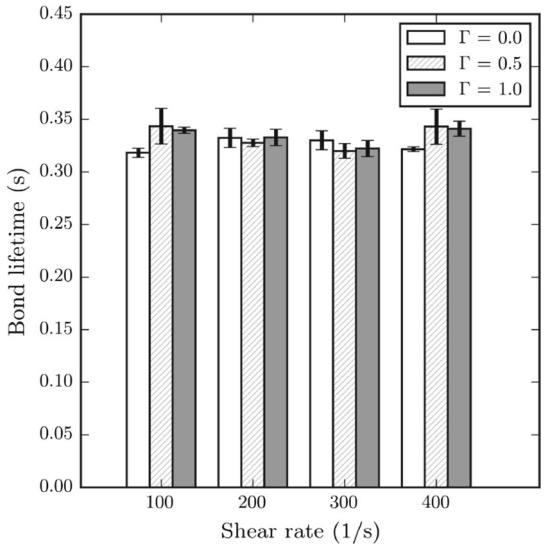

Fig. 14 Influence of strain hardening membrane and shear rate on bond lifetime. The average bond lifetime during capsule rolling on selectin-coated surface was calculated at shear rates of 100 to 400 s^{-1} for Γ values of 0.0, 0.5, and 1.0 (mean ± SE; $n = 5$–7)

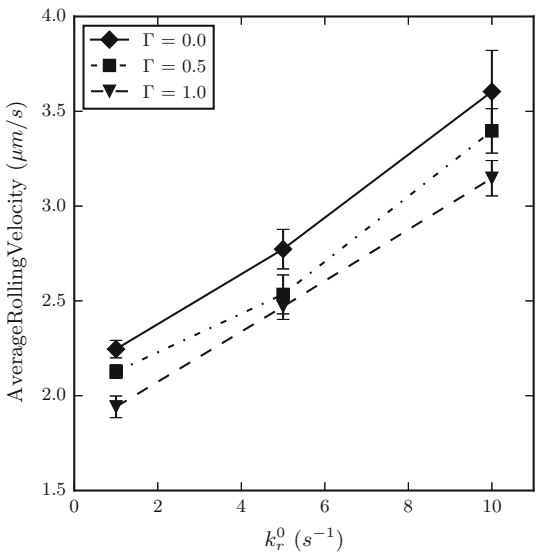

Fig. 15 Effect of unstressed reverse rate constant (off-rate) in the Bell model on the average rolling velocity of the capsules at shear flow of 400 s^{-1}. The average rolling velocity of capsule was calculated at off-rate of 1, 5, and 10 s^{-1} for Γ values of 0.0, 0.5, and 1.0 (mean ± SE; $n = 3$–5)

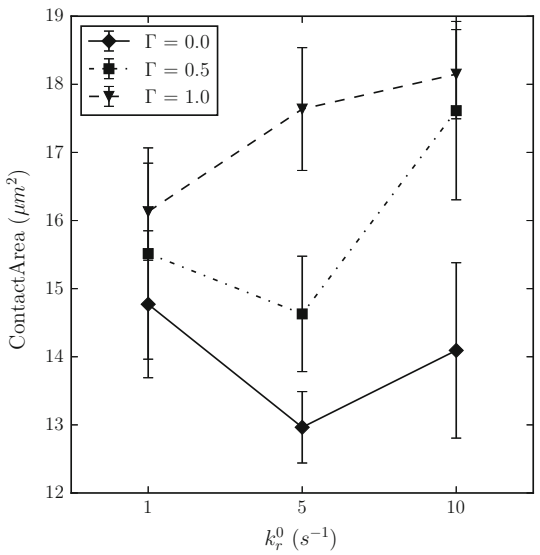

Fig. 16 Average capsule–substrate contact area as a function of the off-rate constant, k_r^0, was estimated from IBM simulations for a deformable capsule rolling under shear flow conditions. The shear rate of 400 s^{-1} for Γ value of 0.0, 0.5, and 1.0 (mean ± SE; $n = 3$–5)

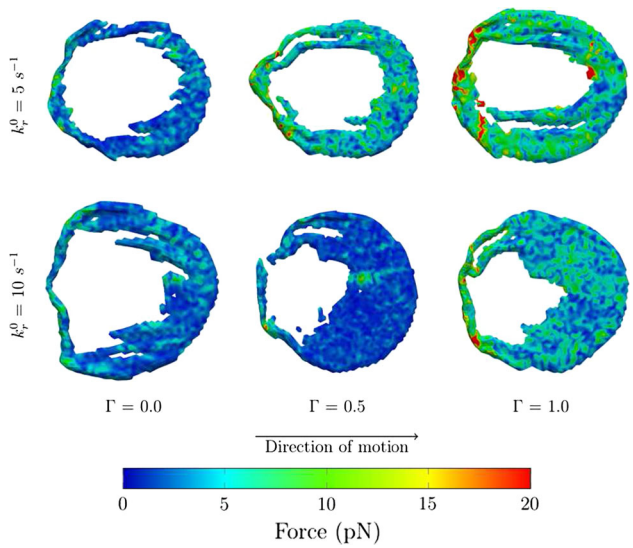

Fig. 17 Contact area shapes at off-rate constant of 5 and 10 s^{-1} are shown for fixed membrane stiffness value (Eh) of 0.3 dyn/cm and shear rate of 400 s^{-1} with varying Γ values of 0.0, 0.5, and 1.0

throughout the simulation compare to a neo-Hookean membrane. Figure 19 shows that higher values of kinetic off-rate caused the bond lifetime to decrease.

4 Discussion

In the present study, the deformation index (L/H) is significantly higher for capsules with a neo-Hookean membrane (i.e. $\Gamma = 0$) at higher shear rate. These results agreed with the reported deformation index (L/H) values for the leukocyte, modeled as neo-Hookean membrane, where the deformation (L/H) increased from 1.1 to 1.3 for increasing shear rates from 100 to 400 s^{-1} (Jadhav et al. 2005; Pappu et al. 2008). In addition, the simulations performed in the current study also revealed that for higher or increasing degree of strain hardening (i.e. $\Gamma > 0$), the capsules exhibited lower deformation at a given shear rate. However, there is a higher variance in deformation index for the capsules with the value of Γ equal

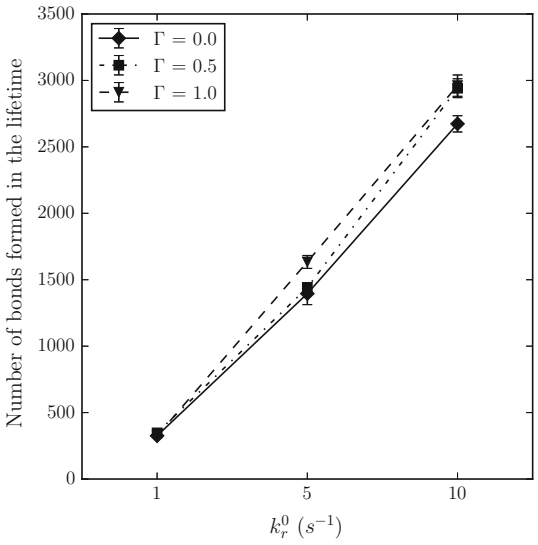

Fig. 18 Effect of unstressed reverse rate constant (off-rate) in the Bell model on the number of bonds formed in the lifetime at shear flow of 400 s^{-1}. The average number of bonds that formed in the lifetime was calculated at off-rate of 1, 5, and 10 s^{-1} for Γ values of 0.0, 0.5, and 1.0 (mean ± SE; $n = 3$–5)

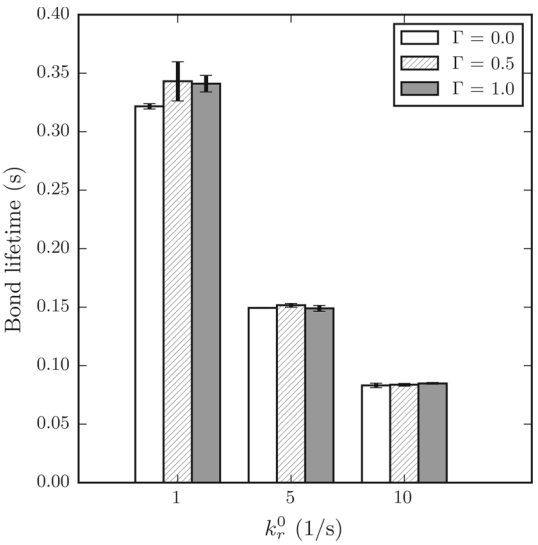

Fig. 19 Effect of unstressed reverse rate constant (off-rate) in the Bell model on the average bond lifetime at shear flow of 400 s^{-1}. The average bond lifetime was calculated at off-rate of 1, 5, and 10 s^{-1} for Γ values of 0.0, 0.5, and 1.0 (mean ± SE; $n = 3$–5)

to zero compared with the other two values for Γ (i.e. Γ at 0.5, 1.0) at shear rate of 400 s^{-1}. This is due in part to the higher hydrodynamic forces exerted on the capsules at shear rate of 400 s^{-1} causing the neo-Hookean capsule to elongate more in the direction of flow as well as the stochastic nature of the receptor–ligand interaction causing the bond lifetime and the number of bonds formed to vary.

In the present study, it was observed that the capsule with the higher second derivative of stress–strain (i.e. $\Gamma = 1.0$) rolled slowly and relatively more smoothly compared to the other values of Γ. Jadhav et al. (2005) and Pappu et al. (2008) studied the influence of membrane stiffness by varying Eh and reported that stiffer membrane deformed less and rolled faster. In the current work, the membrane stiffness, Eh, is fixed at 0.3 dyn/cm and the membranes nonlinear stiffness parameter, Γ, was varied from zero to one. As the Γ value increased, the membrane deformed less and rolled slower. The present results are in direct contrast with the previously published results by Jadhav et al. (2005), who increased the membrane stiffness, Eh, and observed that the more deformable capsules had more contact area and rolled slowly compared to less deformable capsules that had less contact area and rolled faster. This difference in results is due to varying the Γ, which results in membrane having strain hardening behavior and causes the capsule to deform less and not elongate in the direction of the flow as the neo-Hookean membrane (see Fig. 4b). In addition, capsules with the severe strain hardening membrane had higher contact area and less footprint, which led to them not rolling as fast as capsule with less strain hardening membrane that had less contact area and more footprint. The severe strain hardening membrane (i.e. $\Gamma = 1.0$) had smaller dimple size compared to a neo-Hookean membrane (i.e. $\Gamma = 0.0$), which is represented by the empty space in Fig. 8. The most pronounced capsule deformation was for the neo-Hookean ($\Gamma = 0$) membrane at a shear rate of 400 s^{-1}. In addition, the neo-Hookean membrane had less contact area but bigger footprint compared to any other membrane at shear rate of 400 s^{-1}. Even though the less deforming capsule rolled slower, it had higher contact area compared to the faster rolling capsule. The similar behavior was observed between the present study and Jadhav et al. (2005): that is higher contact area resulted in slower rolling.

As the capsule makes contact with the substrate, a thin lubrication fluid layer appears between the capsule and the substrate wall. The lubrication layer is trapped in between the capsule and substrate creating a concave shape on the bottom surface of the capsule, which is called a dimple and represented in Fig. 9.

Dimple formation has been observed for a deformable droplet separated from a solid wall by a thin aqueous film (Platikanov 1964; Connor and Horn 2003; Horn et al. 2006; Zdravkov et al. 2006) and analyzed theoretically (Bart 1968; Quan 2012). In addition, the dimple formation has been simulated for interaction between two deformable particles separated by thin liquid film (Dagastine et al. 2006; Jadhav et al. 2007; Chan et al. 2011) and observed experimentally (Zdravkov et al. 2006; Tufano et al. 2009). The contact surface shape for a synthetic capsule such as polymersomes or leukocyte has not been studied for dimple formation, but it is observed for deformable particle interacting with a solid surface separated by a thin liquid film.

In the present study, the effect of dimple formation on contact area was observed as the degree of membrane strain hardening increased at high shear rate of $400\,s^{-1}$ (see Fig. 6). Thin lubrication fluid layer was observed to push against the capsule from underneath causing it to deform. The strain hardening membrane tends to resist the deformation as shown in Fig. 4a, resulting in the membrane being able to push against the thin fluid layer that is underneath, thus increasing its surface contact with the substrate. The size of the footprint and contact area increased and further results in increase in the average number of bonds.

The value of Γ of the capsule has a strong influence on the dimple size, contact area, rolling velocity, and binding kinetics of the capsule. To increase the rolling velocity of the capsule, it is important that the membrane is elastic-plastic (i.e. $\Gamma = 0.0$). This allows the capsule to elongate in the direction of flow, thus decreasing the bond lifetime (see Fig. 14) compared to the strain hardening membrane. The results show that the increase in bond lifetime hinders the ability of the capsule to role faster.

It was computed that the rolling velocity increases as the kinetic off-rate increases, which was also observed by Krasik and Hammer (2004). One expects the capsule's contact area to decrease as the rolling velocity increased, which was only observed for the neo-Hookean membrane. The strain hardening membrane had more contact area as the rolling velocity increased with increasing off-rate constant. To address this anomaly, the contact surface area was analyzed and it was noticed that as the capsule started to roll faster, the front of the capsule had more surface in contact with the substrate. The strain hardening membrane had more contact area in the front of the capsule, resulting in it having a higher contact area. This allows the capsule to easily break up bonds in the rear and move forward. The strain hardening membrane rolls relatively slower and formed more bonds in the 1s simulation compared to the less strain hardening membrane or neo-Hookean membrane. The further increase in the rolling velocity of the capsule was hindered by the amount of bonds that the capsule formed.

The rolling velocity was also influenced by the capsule membrane where the less strain hardening membrane allows the capsule to elongate in the direction of flow resulting in easier break up of the formed bonds in the rear of the capsule. The strain hardening membrane decreased the deformation index of the capsule for a given shear rate, but the most pronounced difference in the deformation index among the various membrane occurs at shear rate of $200\,s^{-1}$ and above. Additionally, the increasing kinetic off-rate for the Bell model did decrease the bond lifetime allowing the capsule to roll faster.

5 Conclusion

The immersed boundary method (IBM) was implemented to simulate the rolling of a deformable artificial capsule, whose membrane was modeled using the MR strain energy function, on a selectin-coated surface due to shear flow. The MR model was developed to characterize the behavior of elastomers, whose mechanical behavior varies based on degree of cross-linking. In the present work, the capsule's membrane was characterized as strain hardening (Γ) with degree of strain hardening increasing as Γ increased and neo-Hookean ($\Gamma = 0$).

The findings of the present work were: (1) the deformation index (L/H) decreased as the Γ increased for a given shear rate; (2) the contact area between the capsule and substrate increased with the shear rate with the most contact area at the shear rate of $400\,s^{-1}$ for increasing value of Γ; (3) the shape of the contact area and amount of footprint were influenced by the degree of the membranes' strain hardening with the neo-Hookean membrane having higher footprint compared to strain hardening membranes; (4) the rolling of the capsules became relatively smoother and slower as Γ increased; (5) the average number of bonds for a capsule was equivalent for all three values of Γ at a given shear rate; (6) the total receptor–ligand bond force increased with increasing values of Γ; (7) the bond lifetime did not change drastically with increasing shear rate and also with increasing Γ value; and (8) the increasing kinetic off-rate resulted in capsule rolling faster and forming more bonds in a lifetime.

This work analyzed the contact area shape for a deformable membrane rolling on a selectin-coated surface due to shear flow. The slow rolling capsule at shear rate of $100\,s^{-1}$ had most of the contact area located at the rear, while at shear rate of $400\,s^{-1}$, the contact area was evenly spread out. The fast rolling capsule with higher kinetic off-rate had the contact area located on the front of the capsule. As the capsule makes contact with the substrate, a thin lubrication fluid film appears between the capsule and substrate causing the capsule not to be in complete contact with the substrate and produced a dimple. This behavior has been observed and studied by researchers for a deformable droplet separated from a solid wall by a thin aqueous film (Platikanov 1964; Connor and Horn 2003; Horn et al. 2006; Zdravkov et al. 2006; Bart 1968; Quan 2012). In addition, the present work reveals that the capsule membrane's nonlinear material can highly influence the deformation, but there was less pronounced difference for the rolling and adhesion due to strain hardening. In the work by Jadhav et al. (2005) and Pawar et al. (2008), the higher membrane stiffness, Eh, increased the rolling velocity and decreased the deformation. In the present study, the deformation was decreased by increasing the degree of strain hardening, which is achieved through increasing the value of Γ with fixed membrane stiffness, Eh.

Increasing the value of Γ did not have a significant influence on the bond lifetime. Strain hardening capsule's membranes had increased contact area at high shear rate of $400\,s^{-1}$, but it had appreciably less deformation compared to a neo-Hookean membrane. Finally, in the present work the membrane deformation, contact shape, and rolling velocity were influenced by the Γ, strain hardening variable. However, the kinetic off-rate did provided more substantial influence on the rolling velocity and bond lifetime.

The formation of dimple on the capsule can be analyzed experimentally. This can be accomplished by using an inverted microscope in conjunction with a microfluidic channel coated with ligands, where a deformable capsule coated with receptors is under shear flow, to observe the dimple formation. If the dimple was present, the contact surface shape would not be in complete contact with the substrate.

Acknowledgments The hardware used in the computational studies is part of the UMBC High Performance Computing Facility (HPCF). The facility is supported by the US National Science Foundation through the MRI program (Grant Nos. CNS–0821258 and CNS–1228778) and the SCREMS program (Grant No. DMS–0821311), with additional substantial support from the University of Maryland, Baltimore County (UMBC). See www.umbc.edu/hpcf for more information on HPCF and the projects using its resources.

References

Alexeev A, Verberg R, Balazs A (2006) Modeling the interactions between deformable capsules rolling on a compliant surface. Soft Matter 2(6):499–509

Alon R, Ley K (2008) Cells on the run: shear-regulated integrin activation in leukocyte rolling and arrest on endothelial cells. Curr Opin Cell Biol 20(5):525–532

Bart E (1968) The slow unsteady settling of a fluid sphere toward a flat fluid interface. Chem Eng Sci 23(3):193–210

Bell GI (1978) Models for the specific adhesion of cells to cells. Science (New York, NY) 200(4342):618–627

Bermudez H, Brannan AK, Hammer DA, Bates FS, Discher DE (2002) Molecular weight dependence of polymersome membrane structure, elasticity, and stability. Macromolecules 35(21):8203–8208

Caputo KE, Hammer DA (2005) Effect of microvillus deformability on leukocyte adhesion explored using adhesive dynamics simulations. Biophys J 89(1):187–200

Chan DY, Klaseboer E, Manica R (2011) Film drainage and coalescence between deformable drops and bubbles. Soft Matter 7(6):2235–2264

Charrier J, Shrivastava S, Wu R (1989) Free and constrained inflation of elastic membranes in relation to thermoforming-non-axisymmetric problems. J Strain Anal Eng Design 24(2):55–74

Chen S, Springer TA (1999) An automatic braking system that stabilizes leukocyte rolling by an increase in selectin bond number with shear. J Cell Biol 144(1):185–200

Connor JN, Horn RG (2003) The influence of surface forces on thin film drainage between a fluid drop and a flat solid. Faraday Discuss 123:193–206

Dagastine RR, Manica R, Carnie SL, Chan D, Stevens GW, Grieser F (2006) Dynamic forces between two deformable oil droplets in water. Science 313(5784):210–213

Dembo M (1994) On peeling an adherent cell from a surface. Lect Math Life Sci 24:51–77

Devarajan P, Jain S (2015) Targeted drug delivery: concepts and design. Springer

Discher BM, Maloney KM, Grainger DW, Hall SB (2002) Effect of neutral lipids on coexisting phases in monolayers of pulmonary surfactant. Biophys Chem 101–102:333–345

Dong C, Lei XX (2000) Biomechanics of cell rolling: shear flow, cell-surface adhesion, and cell deformability. J Biomech 33(1):35–43

Dore M, Korthuis RJ, Granger DN, Entman ML, Smith CW (1993) P-selectin mediates spontaneous leukocyte rolling in vivo. Blood 82(4):1308–1316

Edwards-Lévy F, Lévy MC (1999) Serum albumin-alginate coated beads: mechanical properties and stability. Biomaterials 20(21):2069–2084

Eggleton C, Popel A (1998) Large deformation of red blood cell ghosts in a simple shear flow. Phys Fluids 10:1834–1845

Fritz J, Katopodis AG, Kolbinger F, Anselmetti D (1998) Force-mediated kinetics of single p-selectin/ligand complexes observed by atomic force microscopy. Proc Natl Acad Sci USA 95(21):12283–12288

Green AE (1970) The fundamental nuclear interaction: important developments of the past decade on mesons and the theory of nuclear forces are described. Science (New York, NY) 169(3949):933–941

Gupta VK, Sraj IA, Konstantopoulos K, Eggleton CD (2010) Multi-scale simulation of L-selectin-PSGL-1-dependent homotypic leukocyte binding and rupture. Biomech Model Mechanobiol 9(5):613–627

Hammer DA, Apte SM (1992) Simulation of cell rolling and adhesion on surfaces in shear flow: general results and analysis of selectin-mediated neutrophil adhesion. Biophys J 63(1):35–57

Hammer DA, Robbins GP, Haun JB, Lin JJ, Qi W, Smith LA, Ghoroghchian PP, Therien MJ, Bates FS (2008) Leuko-polymersomes. Faraday Discuss 139:129–141

Horn RG, Asadullah M, Connor JN (2006) Thin film drainage: hydrodynamic and disjoining pressures determined from experimental measurements of the shape of a fluid drop approaching a solid wall. Langmuir 22(6):2610–2619

Hyduk SJ, Cybulsky MI (2009) Role of alpha4beta1 integrins in chemokine-induced monocyte arrest under conditions of shear stress. Microcirculation 16(1):17–30 (New York, NY : 1994)

Jadhav S, Eggleton CD, Konstantopoulos K (2005) A 3-D computational model predicts that cell deformation affects selectin-mediated leukocyte rolling. Biophys J 88(1):96–104

Jadhav S, Chan KY, Konstantopoulos K, Eggleton CD (2007) Shear modulation of intercellular contact area between two deformable cells colliding under flow. J Biomech 40(13):2891–2897

Khismatullin DB, Truskey GA (2005) Three-dimensional numerical simulation of receptor-mediated leukocyte adhesion to surfaces: effects of cell deformability and viscoelasticity. Phys Fluids (1994-present) 17(3):031,505

Krasik EF, Hammer DA (2004) A semianalytic model of leukocyte rolling. Biophys J 87(5):2919–2930

Lawrence MB, Springer TA (1991) Leukocytes roll on a selectin at physiologic flow rates: distinction from and prerequisite for adhesion through integrins. Cell 65(5):859–873

Lee JS, Feijen J (2012) Polymersomes for drug delivery: design, formation and characterization. J Controll Release 161(2):473–483

Ley K (2009) Leukocyte adhesion, 1st edn. Academic Press, Amsterdam

Magill M (1990) Microencapsulation for the personal care industry. Cosmet Toilet 105(6):59–62

Mehta P, Cummings RD, McEver RP (1998) Affinity and kinetic analysis of P-selectin binding to P-selectin glycoprotein ligand-1. J Biol Chem 273(49):32506–32513

Miyazawa K, Yajima I, Kaneda I, Yanaki T (2000) Preparation of a new soft capsule for cosmetics. J Cosmet Sci 51(4):239–252

Mooney M (1940) A theory of large elastic deformation. J Appl Phys 11:582–592

Moore KL, Varki A, McEver RP (1991) GMP-140 binds to a glycoprotein receptor on human neutrophils: evidence for a lectin-like interaction. J Cell Biol 112(3):491–499

Nimmerfall F, Rosenthaler J (1986) Modified release of drug: a way to its quantification. Int J Pharm 32(1):1–6

Norman KE, Moore KL, McEver RP, Ley K (1995) Leukocyte rolling in vivo is mediated by P-selectin glycoprotein ligand-1. Blood 86(12):4417–4421

Pappu V, Doddi SK, Bagchi P (2008) A computational study of leukocyte adhesion and its effect on flow pattern in microvessels. J Theor Biol 254(2):483–498

Pawar P, Jadhav S, Eggleton CD, Konstantopoulos K (2008) Roles of cell and microvillus deformation and receptor-ligand binding kinetics in cell rolling. Am J Physiol Heart Circ Physiol 295(4):H1439–H1450

Peskin C (1989) A 3-dimensional computational method for blood-flow in the heart. 1 Immersed elastic fibers in a viscous incompressible fluid. J Comput Phys 81(2):372–405

Petri B, Phillipson M, Kubes P (2008) The physiology of leukocyte recruitment: an in vivo perspective. J Immunol 180(10):6439–6446 (Baltimore, Md : 1950)

Platikanov D (1964) Experimental investigation on the dimpling of thin liquid films. J Phys Chem 68(12):3619–3624

Quan S (2012) Dynamics and thin film drainage of a deformable droplet moving towards a solid wall with finite inertia. RSC Adv 2(5):1927–1935

Rachik M, Barthes-Biesel D, Carin M, Edwards-Levy F (2006) Identification of the elastic properties of an artificial capsule membrane with the compression test: effect of thickness. J Colloid Interface Sci 301(1):217–226

Rivlin R (1948) Large elastic deformations of isotropic materials. iv. further developments of the general theory. Philos Trans R Soc Lond A Math Phys Eng Sci 241(835):379–397

Robbins GP, Saunders RL, Haun JB, Rawson J, Therien MJ, Hammer DA (2010) Tunable leuko-polymersomes that adhere specifically to inflammatory markers. Langmuir ACS J Surf Colloids 26(17):14089–14096

Shao JY, Ting-Beall HP, Hochmuth RM (1998) Static and dynamic lengths of neutrophil microvilli. Proc Natl Acad Sci USA 95(12):6797–6802

Smith ML, Smith MJ, Lawrence MB, Ley K (2002) Viscosity-independent velocity of neutrophils rolling on p-selectin in vitro or in vivo. Microcirculation 9(6):523–536 (New York, NY : 1994)

Soda M, Pannell L, Olson N (1989) Microencapsulated enzyme systems for the acceleration of cheese ripening. J Microencapsul 6(3):319–326

Tandon P, Diamond SL (1998) Kinetics of beta2-integrin and l-selectin bonding during neutrophil aggregation in shear flow. Biophys J 75(6):3163–3178

Tözeren A, Ley K (1992) How do selectins mediate leukocyte rolling in venules? Biophys J 63(3):700–709

Tufano C, Peters GW, Van Puyvelde P, Meijer HE (2009) Study of morphological hysteresis in partially immiscible polymers. Rheol Acta 48(3):343–358

Vallner J, Honigberg I, Kotzan J, Stewart J (1983) A proposed general protocol for testing bioequivalence of controlled-release drug products. Int J Pharm 16(1):47–55

Yago T, Wu J, Wey CD, Klopocki AG, Zhu C, McEver RP (2004) Catch bonds govern adhesion through l-selectin at threshold shear. J Cell Biol 166(6):913–923

Zdravkov A, Peters G, Meijer H (2006) Film drainage and interfacial instabilities in polymeric systems with diffuse interfaces. J Colloid Interface Sci 296(1):86–94